J Arid Land (2023) 15(7): 757–778
https://doi.org/10.1007/s40333-023-0062-z

Science Press Springer-Verlag

Correlation analysis between the Aral Sea shrinkage and the Amu Darya River

WANG Min[1,2,3,4,5], CHEN Xi[1,2,4,5,6*], CAO Liangzhong[7], KURBAN Alishir[1,4,5], SHI Haiyang[8], WU Nannan[1], EZIZ Anwar[1], YUAN Xiuliang[1], Philippe DE MAEYER[1,2,3,4,5]

[1] State Key Laboratory of Desert and Oasis Ecology, Xinjiang Institute of Ecology and Geography, Chinese Academy of Sciences, Urumqi 830011, China;
[2] University of Chinese Academy of Sciences, Beijing 100049, China;
[3] Department of Geography, Ghent University, Ghent 9000, Belgium;
[4] Sino-Belgian Joint Laboratory of Geo-Information, Urumqi 830011, China;
[5] Sino-Belgian Joint Laboratory of Geo-Information, Ghent 9000, Belgium;
[6] Research Center for Ecology and Environment of Central Asia, Chinese Academy of Sciences, Urumqi 830011, China;
[7] Jiujiang University, Jiujiang 332000, China;
[8] Hohai University, Nanjing 211100, China

Abstract: The shrinkage of the Aral Sea, which is closely related to the Amu Darya River, strongly affects the sustainability of the local natural ecosystem, agricultural production, and human well-being. In this study, we used the Bayesian Estimator of Abrupt change, Seasonal change, and Trend (BEAST) model to detect the historical change points in the variation of the Aral Sea and the Amu Darya River and analyse the causes of the Aral Sea shrinkage during the 1950–2016 period. Further, we applied multifractal detrend cross-correlation analysis (MF-DCCA) and quantitative analysis to investigate the responses of the Aral Sea to the runoff in the Amu Darya River, which is the main source of recharge to the Aral Sea. Our results showed that two significant trend change points in the water volume change of the Aral Sea occurred, in 1961 and 1974. Before 1961, the water volume in the Aral Sea was stable, after which it began to shrink, with a shrinkage rate fluctuating around 15.21 km^3/a. After 1974, the water volume of the Aral Sea decreased substantially at a rate of up to 48.97 km^3/a, which was the highest value recorded in this study. In addition, although the response of the Aral Sea's water volume to its recharge runoff demonstrated a complex non-linear relationship, the replenishment of the Aral Sea by the runoff in the lower reaches of the Amu Darya River was identified as the dominant factor affecting the Aral Sea shrinkage. Based on the scenario analyses, we concluded that it is possible to slow down the retreat of the Aral Sea and restore its ecosystem by increasing the efficiency of agricultural water use, decreasing agricultural water use in the middle and lower reaches, reducing ineffective evaporation from reservoirs and wetlands, and increasing the water coming from the lower reaches of the Amu Darya River to the 1961–1973 level. These measures would maintain and stabilise the water area and water volume of the Aral Sea in a state of ecological restoration. Therefore, this study focuses on how human consumption of recharge runoff affects the Aral Sea and provides scientific perspective on its ecological conservation and sustainable development.

Keywords: Aral Sea shrinkage; recharge runoff; Amu Darya River; Syr Darya River; multifractal detrend cross-correlation analysis (MF-DCCA); Bayesian Estimator of Abrupt change, Seasonal change, and Trend (BEAST); Central Asia

Citation: WANG Min, CHEN Xi, CAO Liangzhong, KURBAN Alishir, SHI Haiyang, WU Nannan, EZIZ Anwar, YUAN Xiuliang, Philippe DE MAEYER. 2023. Correlation analysis between the Aral Sea shrinkage and the Amu Darya River. Journal of Arid Land, 15(7): 757–778. https://doi.org/10.1007/s40333-023-0062-z

*Corresponding author: CHEN Xi (E-mail: chenxi@ms.xjb.ac.cn)
Received 2023-01-30; revised 2023-05-22; accepted 2023-05-27

1 Introduction

Water is an important environmental factor and natural resource that plays a crucial role in natural ecosystems, agricultural production, and human well-being. However, freshwater systems, including rivers, lakes, and springs, are directly or indirectly subjected to human influence through land cover change and anthropogenic climate change (Chen et al., 2019; Konapala et al., 2020). This has led to severe consequences, such as the alteration of waterways and the desiccation of rivers and lakes, resulting in ecological and environmental problems including water pollution, ecosystem destruction, habitat loss, etc. For instance, studies have reported that approximately 20% of freshwater lakes have become desiccated, while the altered volume has decreased by over 40% during the last century (Feng et al., 2022), causing 18% of the world's population to face water shortage challenges (Berdugo et al., 2022). Considering the rapid expansion of global drylands (Huang et al., 2016) and population growth (Fróna et al., 2021), these problems are likely to continue and even be exacerbated in the future (Wang et al., 2018; Woolway et al., 2020; Grant L et al., 2021). Because of their severity, the sustainable use of water resources has been added to the UN sustainable development goals (Foster, 2018). As water resources are vulnerable to the harmful impacts of climate change, water shortage and desiccation are especially more pronounced in arid lands owing to low per capita natural resources and inadequate basic infrastructure and water-saving technology in agriculture.

Central Asian is the world's largest arid region, of which the water system mainly includes glacier-fed surface runoff and groundwater. Owing to the intensive overexploitation of water resources and the increase in evaporation and rapid glacier retreat during the past century due to climate change, Central Asia has suffered from severe water shortage, leading to serious environmental problems, including desert expansion, soil salinization, sand storm occurrence, and water pollution (Zhang et al., 2019; Pham-Duc et al., 2020; Hu et al., 2022). Consequently, according to a recent report by Li et al. (2022), soil salinization and desertification-related economic losses are as high as 3.0×10^{10} USD, posing a serious threat to the food security and sustainable development of the region.

Inland water systems, such as terminal lakes, are essential for maintaining ecosystem stability and regional safety. The desiccation of lakes has a detrimental effect on the natural environment and local population. For example, the Lop Nur Lake desiccation has led to a substantial expansion of the sandy desert, the disappearance of small oases, the complete destruction of the regional ecosystem, and severe soil salinization (Cai et al., 2022). To prevent similar catastrophes, understanding lake distribution and variation in Central Asia and their underlying mechanisms has been a common area of interest in climatic, hydrologic, ecologic, and geographic research (Bai et al., 2012; Liu et al., 2019). As the largest inland terminal lake in arid Central Asia, the Aral Sea plays a key role in the ecological environment and water resource utilisation. However, along with population growth, the rapid expansion of croplands in the middle and upper reaches of the Amu Darya River and Syr Darya River (Rufin et al., 2022), which represent the main water sources of the Aral Sea, has significantly decreased the incoming water to the lake basin. In addition, over the past 100 years, glacial recession and an increase in evapotranspiration caused by global warming have exacerbated the severity of this problem in Central Asia (Wang et al., 2020). Furthermore, the construction of hydrological infrastructure, such as hydropower stations built in Tajikistan, Uzbekistan, and Kyrgyzstan in the upper reaches of the Amu Darya River and Syr Darya River, and water drainage channels, including the Karshi Canal, Karakum Channel, and Amu-Bukhara Canal, have also reduced the water flow into the lake. Moreover, a lack of unified systematic monitoring, management, and planning measures for water resources and agricultural lands—especially after the collapse of the Soviet Union—has led to excessive land reclamation, overexploitation of groundwater, and inappropriate irrigation, causing a reduction in the runoff volume of rivers, the decline of the water table, and secondary salinization (Liu et al., 2022). Consequently, in 1951, 6.600×10^{4} km^3 of the water surface area of the Aral Sea, which was previously used to support local fishery, was divided into four separate water patches spanning

7.000×10^3 km^3 today (Wu et al., 2022), creating large swathes of saline islands and sandy deserts around and in the middle of the lake basin. This has led to the desiccation of the local climate, causing frequent heatwaves and sandstorms that pose serious threats to socioeconomic development and even the health and well-being of the local population (Sharma et al., 2018; He et al., 2022).

Thus, understanding the hydrological and anthropogenic processes that caused lake desiccation in order to find a way to mitigate it is one of the main focuses of dryland research. For instance, research conducted by Huang et al. (2022) and Zhang et al. (2022), who analysed glacier changes over the past century, showed that the inland lakes in Central Asia decreased, while the higher-altitude alpine lakes increased significantly along with glacier meltwater, stressing the importance of human activities in the lake area reduction of the Aral Sea. Rufin et al. (2022) reported that croplands increased from 4.400×10^4 km^2 in 1987 to 5.200×10^4 km^2 in 2017, with more than a 200% increase in double-cropping irrigation lands, followed by a rapid urban expansion and sharp rise in water consumption in the last 20 years (Yan and Li, 2023), contributing to the problem. A comparative analysis of climatic and anthropogenic factors by Yang et al. (2020a) concluded that anthropogenic factors were the main cause of the reduction in the lake area. Even though these studies have deepened our understanding of the relative contributions of climatic and anthropogenic factors to some extent, the ways in which specific hydrological and human-driven processes of the major water sources of the lake have led to the lake area reduction of the Aral Sea remain unclear. As a major water source, the Amu Darya River has considerable influence on the lake area fluctuations. Human activities or water volume fluctuations in any reach of the Amu Darya River could directly affect the lake area variation. However, the effect of runoff variations in the Amu Darya River on Aral Sea water area fluctuations is still mostly unknown. Therefore, analysing the response of the Aral Sea's water volume and lake area to the runoff variations of the Amu Darya River would help us to understand the mechanisms behind the shrinkage of the Aral Sea. Further, it would provide a scientific basis for local authorities to improve their water resource management regime and halt the continued devastation of the region's natural environment.

In general, parametric (e.g., cumulative anomaly and sliding *t*-test) and non-parametric (e.g., Mann-Kendall test, Pettitt's test, and Bayesian analysis) methods (Hrvatin and Zorn, 2022) are widely used for detecting the change-point in surface runoff as well as the corresponding water volume and lake area. These methods are easy to operate and can deliver relatively robust results when observation data are sufficient and the relationship between the explanatory factors of the lake area and volume variation appears to be relatively simple (Alkan and Konukcu, 2022). As most of these methods are based on statistical parameters, such as Akaike's information criterion and the Bayesian information criterion (Hrvatin and Zorn, 2022), their produced results do not always align with each other and can even be contradictory (Zhao et al., 2019). Conventional methods may not necessarily perform well when analysing complex hydrological processes. A holistic approach based on the direct and indirect hydrological processes of river networks has been proven to more realistically reflect the underlying mechanisms of lake variation (Zhao et al., 2004). In this study, we used a novel approach for hydrological analysis—the Bayesian Estimator of Abrupt change, Seasonal change, and Trend (BEAST) model—to explore this relationship. As the BEAST model comprehensively ensembles various competing models based on the Bayesian approach, it can effectively help explore intrinsic causal relations in terms of the dimension of temporal dynamics (Zhao et al., 2019). Other popular change-point detection methods are based on other single values, such as the mean and variance (Pettitt, 1979; Vinushree et al., 2022; Banakara et al., 2023), which are often unable to precisely find change-points, leading to a contradiction in the explanatory factors.

Furthermore, we used the multifractal detrend cross-correlation analysis (MF-DCCA) method to explore the complex non-linear relationships between the hydrological variables in this study; the MF-DCCA method shows some advantages in handling the non-linear interaction relations between non-stationary time series, which has been widely applied in finance but rarely used in

hydrology. This method discerns the non-linear dynamic pattern of each variable by both studying the multifractal features of the variable sequence and calculating the long-range correlation of the variable obtained by varying the time-scale of the Hurst index (Xiang et al., 2019; Rahmani and Fattahi, 2021; Yang et al., 2021; Kojić et al., 2022).

Based on these considerations, the surface runoff data from the hydrological monitoring stations along the Amu Darya River, and the satellite-driven water level, water area, and water volume data of the Aral Sea from 1950 to 2016, we analysed the effect of Amu Darya River runoff variations on the Aral Sea fluctuations to provide new insights and a scientific basis for sustainable water use and management in the region. Specifically, we addressed the following questions:

(1) What are the dynamics of the Aral Sea and the surface runoff and water consumption of the Amu Darya River during 1950–2016?

(2) What are the reasons for the Aral Sea shrinkage, and do they vary with time?

(3) How does the Amu Darya River runoff affect the water volume of the Aral Sea during the study period?

Analysing the connection between the Aral Sea shrinkage and the Amu Darya River will not only clarify the role of human activities in the evolution of rivers and lakes in the arid zone of Central Asia, but also provide a scientific basis for the rational development and protection of water resources and the promotion of regional sustainable development.

2 Data and methods

2.1 Study area

The Aral Sea (58°–62°E, 43°–47°N) is located in Central Asia, at the border of the Republic of Karakalpakstan in Uzbekistan and the Kyzylorda and Aktobe oblasts in Kazakhstan. It meets the delta of the Syr Darya River to the north and the delta of the Amu Darya River to the south, with a high topography in the west and a low one in the east (Fig. 1). The Aral Sea region is characterised by an extreme continental climate. Precipitation is higher in April and October (with a daily amount of 0.48 mm) and lower in August and September (with a daily amount of approximately 0.22 mm). Temperature is higher in summer (with a monthly average value of 25°C and a monthly maximum value of 47°C) and lower in winter (with a monthly average temperature of –11°C and a monthly minimum temperature of –38°C). Annual evaporation is as high as 1700 mm. As a terminal lake in an arid zone in Central Asia, runoff from the Amu Darya River and Syr Darya River is the largest source of its recharge.

The Aral Sea was once the second largest inland saltwater lake in Asia after the Caspian Sea and the fourth largest lake in the world. In the 1950s, the Aral Sea had a water area over 7.000×10^4 km^2, an average altitude of 53 m, a maximum length of 435 km from north to south, a width of 290 km from east to west, an average depth of 16 m, a maximum depth of 69 m on the west bank, and a total water volume of approximately 1.000×10^4 km^3 (Micklin, 1988, 2007, 2010, 2016; Micklin and Aladin, 2008). In the 1960s, the Aral Sea covered an area of approximately 6.500×10^4 km^2, but its area decreased year by year, splitting into the South Aral Sea (Big Aral Sea) and North Aral Sea (Small Aral Sea) in 1986, with the Big Aral Sea further splitting into the East Aral Sea and West Aral Sea in 2007. The lake area has now been reduced to approximately 0.400×10^4 km^2, with the elevation of the lake surface in the West Aral Sea dropping to 26 m, while the Small Aral Sea remains above 40 m, and the total water volume of the lake has dropped to about 50.000 km^3. Overall, the Aral Sea has shrunk rapidly since the 1960s, with its lake area now being less than 10% of its previous size, leading to huge impacts on the local ecological environment and social economy.

2.2 Data sources

The data used in this study mainly include lake data from the Aral Sea (before 1986) and Big Aral Sea (after 1986), hydrological data from the Amu Darya River and Syr Darya River, and

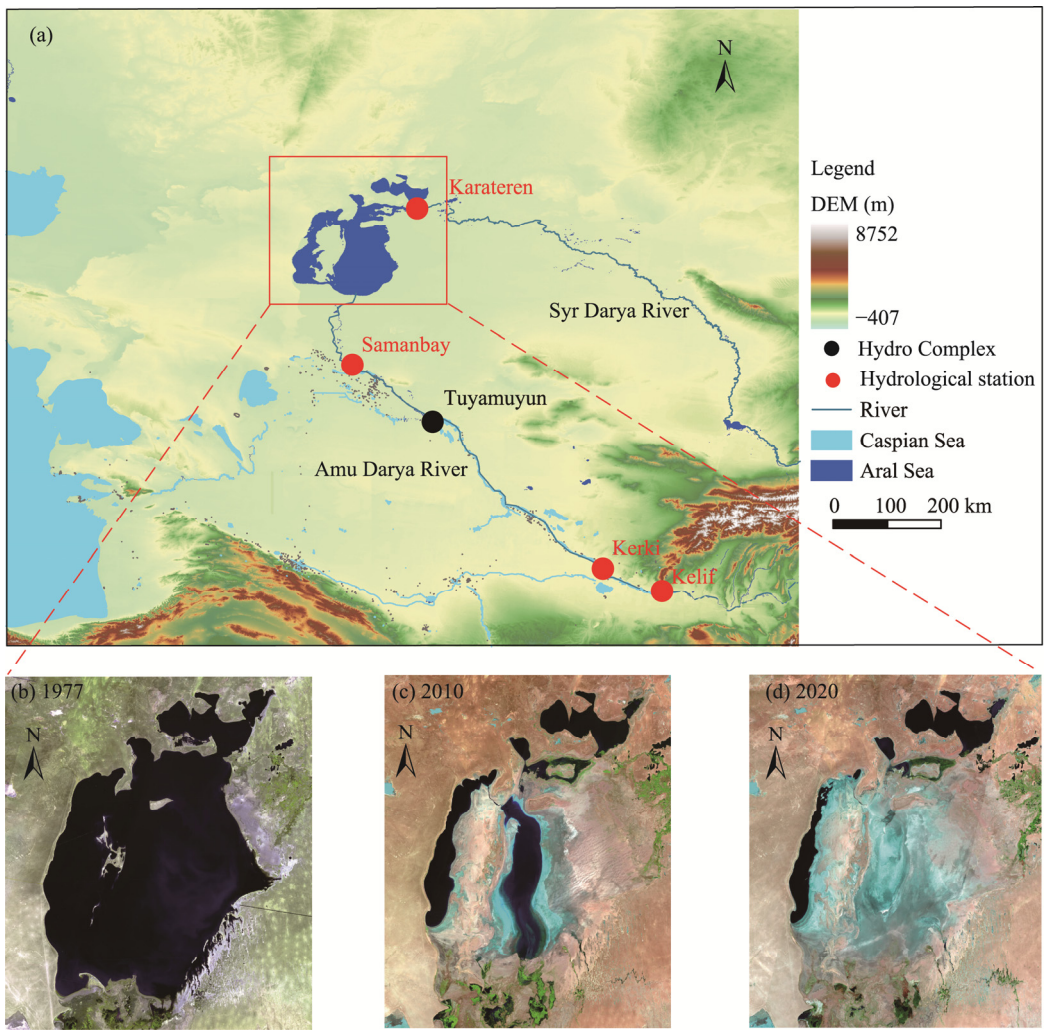

Fig. 1 Overview of the Aral Sea region in Central Asia (a) and MODIS images showing the lake area variations of the Aral Sea in 1977 (b), 2010 (c), 2020 (d). MODIS images are derived from National Aeronautics and Space Administration (NASA) (https://www.earthdata.nasa.gov/sensors/modis).

socioeconomic data from the Aral Sea, which are all annual data. The lake data, obtained from the CA Water website (http://www.cawater-info.net/), comprise the water level, water area, and water volume during the 1950–2017 period and the theoretical capacity of the Aral Sea.

The hydrological data include the *in-situ* runoff data (1950–2016) from four hydrological stations located in the upper, middle, and lower reaches of the Amu Darya River (Kelif, Kerki, and Samanbay hydrological stations, respectively) and the lower reaches of the Syr Darya River (Karateren hydrological station, denoted by the symbol Syr_Down). Additionally, they include the reservoir storage capacity (1983–2017) of the Tuyamuyun Hydro Complex (THC), which is located at the beginning of the lower Amu Darya River, between the Kerki and Samanbay hydrological stations, and is the sole and largest reservoir in the downstream area, with a total capacity of 6.900–7.800 km^3.

2.3 Correction of the lake data

Because of inconsistencies in the original historical annual data, their direct use leads to distorted results and unsatisfactory simulations. These inconsistencies are mainly rooted in two aspects: (1) the correspondence between the three types of lake data (water level, water area, and water volume) fails to follow the theoretical capacity curve and (2) the inconsistency between these lake

datasets in their temporal fluctuations. This is attributed to the inconsistency of temporal data we obtained, as the Aral Sea fluctuated greatly within an annual scale, and its water volume values varied greatly among different months. In addition, the raw data were prone to errors in the process of being recorded, and the raw data were not collected at the same or similar times. Therefore, we developed an analytical procedure to derive the most suitable time series data using a combination of mapping based on theoretical capacity curves and optimisation techniques, as described in Figure 2.

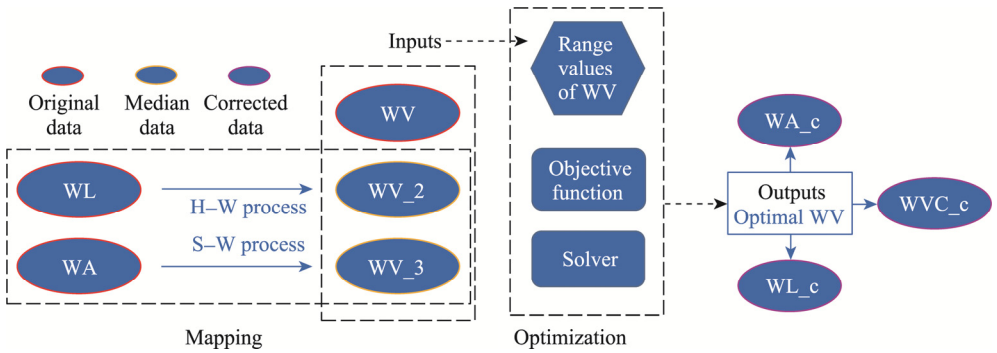

Fig. 2 Flow chart of the lake data correction in this study. WV, WL, and WA represent the water volume, water level, and water area, respectively; WV_2 and WV_3 represent the transformed water volume under the two transformation methods, respectively; WA_c, WL_c, and WVC_c represent the corrected water area, water level, and water volume change, respectively; H–W process and S–W process represent the inversion of the water level–water volume relation and the inversion of the water area–water volume relation, respectively.

In this study, we focused on the water volume data and its changes. The sets of original annual water level and water area data for the Big Aral Sea from 1950 to 2017 were first mapped into the water volume data using the theoretical capacity curves. Through mapping, we obtained three types of the water volume data: the original data, the transformed data obtained by the inversion of the water level–water volume relation (H–W process), and the transformed data obtained by the inversion of the water area–water volume relation (S–W process). The Aral Sea was split into the Small Aral Sea and Big Aral Sea in 1986, while the latter was further split into the East Aral Sea and West Aral Sea in 2007. We fit the water level–water area–water volume relationship with polynomials and considered those in three segments corresponding to three periods in history: 1950–1985, 1986–2006, and 2007–2017. Finally, we obtained several sets of water volume data from 1950 to 2017, constituting a range of values. We selected the most suitable single values for the follow-up study from the range of values constituted by the available water volume data using optimisation techniques, whose essence lies in the temporal inconsistency of the data. As it is difficult to obtain long time series data that are mostly consistent over time, optimisation techniques are useful and necessary. During the optimisation, the constrained non-linear minimisation solver was used to minimise the negative correlation between the water volume change and its recharge runoff. Using the interior point algorithm and 355 iterations, we obtained the final water volume data. As for the runoff recharge, the downstream recharge of the Amu Darya River and Syr Darya River was combined before 1986, after which only the downstream recharge of the Amu Darya River was considered, with the corresponding water volume change from the Big Aral Sea. As the shrinkage of the Aral Sea mainly occurred in the Big Aral Sea during 1986–2017, the Small Aral Sea was isolated from the Big Aral Sea, with the water volume increasing steadily. Using the theoretical capacity curves, the corresponding corrected water level and water area data were obtained by the inversion of the corrected water volume data.

2.4 Sen's slope calculation

Sen's slope calculates the slope (i.e., the linear rate of change) and confidence level (Pohlert, 2016), according to the following equations:

$$d_{ij} = \frac{x_j - x_i}{t_j - t_i} (1 \le i < j \le N), \tag{1}$$

$$b_{\text{sen}} = \text{median}(d), \tag{2}$$

where d_{ij} is the slope calculated between the two time points t_i and t_j; x_i and x_j are the corresponding values of the variables at time points t_i and t_j, respectively; N is the length of the data; b_{sen} is the Sen's slope; and d is the set of all slopes with a total number of $N(N–1)/2$.

2.5 Multifractal detrend cross-correlation analysis (MF-DCCA) method

The MF-DCCA method proposed by Zhou (2008) is based on the multifractal detrended fluctuation analysis and detrended cross-correlation analysis (DCCA) methods. It mainly includes the following steps. First, by assuming that two non-stationary sequences $x(u)$ and $y(u)$ have the same length N (where u=1, 2, …, N), we constructed two new sequences $X(l)$ and $Y(l)$ (l=1, 2, …, N) according to Equation 3:

$$X(l) = \sum_{u=1}^{l} \left(x(u) - x' \right); \; Y(l) = \sum_{u=1}^{l} \left(y(u) - y' \right), \tag{3}$$

where l is the index for each variable in the new sequences X and Y; and x' and y' represent the mean values of the time series $x(u)$ and $y(u)$, respectively.

Next, the new sequences $X(l)$ and $Y(l)$ were divided into N_s equal-length and non-overlapping sub-intervals, with N_s=int[N/s], where s represents the length of the sub-intervals (i.e., timescale) and N_s is the total number of sub-intervals. Because the timescale s may not be an integer multiple of N, the time series were again segmented from back to forward, with $2N_s$ sub-intervals for every time series. To obtain the fluctuation function of order q, we averaged the detrended variance for all sub-intervals. When q=0, the formula was derived from L'Hôpital's rule:

$$F_q(s) = \left\{ \frac{1}{2N_s} \sum_{v=1}^{2N_s} \left[F^2(s,v) \right]^{q/2} \right\}^{1/q} \quad q \ne 0, \tag{4}$$

$$F_0(s) = \exp\left\{ \frac{1}{4N_s} \sum_{v=1}^{2N_s} ln\left[F^2(s,v) \right] \right\} \; q = 0, \tag{5}$$

where $F_q(s)$ is the fluctuation function of order q when the sub-interval's length is s; $F_0(s)$ is the fluctuation function when q=0; v is the index for each sub-interval; and $F^2(s,v)$ is the detrended variance function of each sub-interval, which is computed by calculating the variance removing the local trend obtained by the least-squares fitting of each sub-interval, as shown in Equations 4 and 5. When v=1, 2, 3, ..., N_s, then

$$F^2(s,v) = \frac{1}{s} \sum_{\tau=1}^{s} \left\{ \left| X\left[(v-1)s + \tau \right] - X_v(\tau) \right| \left| Y\left[(v-1)s + \tau \right] - Y_v(\tau) \right| \right\}, \tag{6}$$

and when v=N_s+1, N_s+2, N_s+3, ..., 2N_s, then

$$F^2(s,v) = \frac{1}{s} \sum_{\tau=1}^{s} \left\{ \left| X\left[N - (v - N_s)s + \tau \right] - X_v(\tau) \right| \left| Y\left[N - (v - N_s)s + \tau \right] - Y_v(\tau) \right| \right\}. \tag{7}$$

Here, $X_v(\tau)$ and $Y_v(\tau)$ are the local trends in each sub-interval, and τ is the index of each variable in the sub-interval (τ =1, 2, …, s). We repeated the described steps using different values of q and examined how $F_q(s)$ changed with timescale s by observing the double log plot between $F_q(s)$ and s. When a power-law cross-correlation exists, the relation satisfies the following formula:

$$F_q(s) \sim s^{h_{x,y}(q)}, \tag{8}$$

where $s^{h_{x,y}(q)}$ represents the function of the timescale s, and $h_{x,y}(q)$ is a specific exponent called the generalized Hurst exponent. When q=2, the MF-DCCA becomes the DCCA. If $h_{x,y}(2)$=0.5, no cross-correlation exists between the two time series. If $h_{x,y}(2)$>0.5, then a forward long-range

cross-correlation exists; whereas if $h_{x,y}(2)<0.5$, an inverted long-range cross-correlation is observed between the two time series. The multifractal features of a time series can be expressed by the dependence of $h_{x,y}(q)$ on q, whereas the monofractal data $h_{x,y}(q)$ are independent of the relative q values. When $q>0$, the generalised Hurst exponent $h_{x,y}(q)$ describes the scale effect of large fluctuations, whereas when $q<0$, $h_{x,y}(q)$ characterizes the scale effect of small fluctuations.

2.6 Bayesian Estimator of Abrupt change, Seasonal change, and Trend (BEAST) model

The BEAST model was developed to isolate periodic and trend signals from a time series and pinpoint abrupt shifts by fitting a Bayesian regression model to match the time series data (Zhao et al., 2019). A time series $D=\{t_u, y_u\}$ (where t_u is the time of each observation; y_u is the observed value at time t_u; and u is the index for each observation (u=1, 2, ..., N)) is believed to comprise three components (seasonality, trend, and mutation plus noise), which can be expressed using the following formula:

$$y_u = S(t_u;\Theta_S) + T(t_u;\Theta_T) + \varepsilon_u . \tag{9}$$

Here, the noise ε_u is assumed to be Gaussian, with a magnitude σ, and the rest of the data are explained by the seasonal $S(t_u; \Theta_S)$ and trend $T(t_u; \Theta_T)$ signals (where Θ_S is the parameter of the seasonal signals; and Θ_T is the parameter of the trend signals). The general linear model was utilised to parameterise $S(t_u; \Theta_S)$ and $T(t_u; \Theta_T)$. The mutation point (i.e., change point) is implied in the Θ_S and Θ_T parameters.

For formulation purposes, the Θ_T and Θ_S parameters were reclassified into two sets, i.e., $\{\Theta_T, \Theta_S\}=\{M, \beta_M\}$. The first set, M, refers to the model structure, including the number and time of the seasonal and trend change points and the seasonal harmonic order. The second set, β_M, is the coefficient parameter of a particular segment used to determine the exact trend shape and seasonal curves after a given model structure M. After recombination, the original general linear model formula becomes:

$$y(t_u) = X_M(t_u)\beta_M + \varepsilon_u , \tag{10}$$

where $y(t_u)$ is the observed value at time t_u; and $X_M(t_u)$ is the dependent variable at time t_u. This equation was extended to a general linear model to create a Bayesian model used to detect sudden changes, seasonality, and trends from the time series data. In the Bayesian modelling, all unknown parameters were considered as random, including the model structure M, the coefficient β_M, and the data noise σ^2. In a given time series $D=\{t_u, y_u\}$, it is necessary to both calculate the best parameter values and obtain their posterior probability distribution $p(\beta_M, \sigma^2, M|D)$, which is the product of a likelihood function and a prior model:

$$p(\beta_M,\sigma^2,M \mid D) \propto p(D \mid \beta_M,\sigma^2,M) \times \pi(\beta_M,\sigma^2,M) , \tag{11}$$

where D is the observed data; $p(D|\beta_M, \sigma^2, M)$ is the probability of observing the data D given the model parameters β_M, σ^2, and M; and $\pi(\beta_M, \sigma^2, M)$ is the prior distribution of the model parameters.

The posterior probability distribution $p(\beta_M, \sigma^2, M|D)$ contains all the necessary information to infer the dynamic features of the system, including trends, seasonal changes, and mutations. The Markov chain Monte Carlo (MCMC) sampling method was used to achieve posterior inference. The study utilised a mixed sampling algorithm to embed the reverse-jump MCMC sampler into the Gibbs' sampling framework, as detailed in Zhao et al. (2019).

2.7 Quantitative analysis of the impact of the Amu Darya River on the Aral Sea's water volume

To quantify the runoff effects of the Amu Darya River on the water volume of the Big Aral Sea, we built a model according to a combination of the water balance equation, multiple regression, and polynomial fitting. First, based on the water balance equation and the closed characteristics of the Aral Sea region, we assumed that the amount of the water volume change equalled to the total evapotranspiration minus the total recharge, as expressed in Equation 12:

$$\mathrm{WVC}=(\mathrm{Eva}-\mathrm{Pre})\times \mathrm{WA} - g(R) , \tag{12}$$

where WVC is the water volume change (km^3/a); Eva is the evaporation (mm); Pre is the precipitation (mm); and WA represents the water area (km^2), and when WA is multiplied by the difference between evaporation and precipitation, the net evaporation (i.e., the expense item) can be obtained. The income term, including various forms of runoff recharge distributed in different spatial locations, can then be considered a function of the runoff of the supply river, defined by $g(R)$. Water volume change, which is equal to the difference between the water volume at a given time m (WV_m; km^3) and the water volume at a subsequent time m+1 (WV_{m+1}; km^3), represents the water volume variation of the lake body; the (–) sign indicates a decreasing water volume (i.e., shrinkage), while the (+) sign indicates an increasing water volume (i.e., expansion).

When the difference between evaporation and precipitation is assumed to be constant or have a small variation and the efficiency of the runoff recharge is constant over a certain time range, the calculation of the magnitude of the water volume change can be converted into a linear simulation of variables water area and recharge runoff from river n (R_n; km^3) using the multiple regression method. Equation 12 was, thus, converted into Equation 13, and the corresponding coefficients α and β could be estimated using the least squares method:

$$\mathrm{WVC}=\alpha\times\mathrm{WA}-\sum\nolimits_n \beta_n\times R_n \ . \tag{13}$$

Furthermore, water area is a function of water volume, also called storage, as expressed in Equation 14. Because they are determined by the topographic features of the same lake basin, there exists a one-to-one correspondence between the water area and water volume. To continue combining Equations 13 and 14, we obtained the piecewise function in Equation 15:

$$\mathrm{WA}=f(\mathrm{WV}), \tag{14}$$

$$\mathrm{WVC}=\begin{cases}\alpha_1\times f_1(\mathrm{WV})-\beta_{11}\times R_1-\beta_2\times R_2, \mathrm{WV}\in \mathrm{WV}_1\\ \alpha_1\times f_2(\mathrm{WV})-\beta_{11}\times R_1-\beta_2\times R_2, \mathrm{WV}\in \mathrm{WV}_2\\ \alpha_2\times f_3(\mathrm{WV})-\beta_{12}\times R_1, \mathrm{WV}\in \mathrm{WV}_3\\ \alpha_2\times f_4(\mathrm{WV})-\beta_{12}\times R_1, \mathrm{WV}\in \mathrm{WV}_4\end{cases}, \tag{15}$$

where R_1 represents the recharge runoff from the Amu Darya River (km^3), for which runoff data from the Samanbay hydrological station were used, while R_2 denotes the recharge runoff from the Syr Darya River (km^3), for which the runoff data from the Karateren hydrological station were utilised. There are four main segments in Equation 15 that are determined by three important time points (1966, 1986, and 2007) in the historical period when the Aral Sea underwent dramatic changes. Before 1986, the Aral Sea was simultaneously recharged by the Amu Darya River and Syr Darya River; however, after 1986, the Aral Sea receded into the Big Aral Sea, which was recharged almost exclusively by the Amu Darya River. Thus, WV_1, WV_2, WV_3, and WV_4 represent the water volume separately during the periods of 1950–1965, 1966–1985, 1986–2006, and 2007–2016; f_1, f_2, f_3, and f_4 represent the function describing the correspondence between the water area and water volume separately during the four periods; and α_1, α_2, β_{11}, β_{12}, and β_2 are the coefficients.

The downstream runoff from the Amu Darya River can also be reflected by the water used in the middle-upper reaches (C_1; km^3), water used in the middle-lower reaches (C_2; km^3), upstream-originating flow (U; km^3), and water storage in the reservoir of the THC (RV; km^3), as described in Equation 16. To continue studying the influence of factors, such as the water used in each river section of the Amu Darya River, on the Big Aral Sea, we constructed piecewise Equation 17. Owing to the properties of the multiple regression method, we chose the used water as independent variable instead of runoff whenever possible, to avoid multi-collinearity.

$$R_1=h(C_1,C_2,U,RV), \tag{16}$$

$$\mathrm{WVC}=\begin{cases}\alpha_3\times f_3(\mathrm{WV})-\gamma_1\times C_1-\gamma_2\times C_2-\gamma_3\times U-\gamma_4\times RV, \mathrm{WV}\in \mathrm{WV}_3\\ \alpha_3\times f_4(\mathrm{WV})-\gamma_1\times C_1-\gamma_2\times C_2-\gamma_3\times U-\gamma_4\times RV, \mathrm{WV}\in \mathrm{WV}_4\end{cases}, \quad (17)$$

where α_3, γ_1, γ_2, γ_3, and γ_4 are the coefficients. Here, the formula is divided into two segments corresponding to the stages before and after the Big Aral Sea split in 2007. As the THC reservoir was built in 1983, the water storage in the reservoir of the THC operated throughout the Big Aral Sea period.

2.8 Set of variables

Characterising the temporal dynamics of the water volume change may not only help understand the manner in which the water volume in the Aral Sea changed during the study period but also help explore the relationship between the water volume and its recharge runoff more directly and effectively in terms of the water balance equation. Therefore, this study chose the water volume change and the following variables related to its recharge runoff for this study: the runoff from the downstream of the Syr Darya River (Syr_Down_R), the runoff from the downstream of the Amu Darya River (Samanbay_R), the water consumption in the middle-upper reaches of the Amu Darya River (obtained by subtracting the runoff at the Kelif hydrological station from Kerki hydrological station (K-K)), the water consumption in the middle-lower reaches of the Amu Darya River (obtained by subtracting the runoff at the Kerki hydrological station from Samanbay hydrological station (K-S)), the water storage in the THC (THC_V), the runoff from the midstream of the Amu Darya River (Kerki_R), and the upstream-originating flow of the Amu Darya River (Kelif_R). Compared to other variables located in the Amu Darya River (from 1950 to 2016), the time series of Syr_Down_R was shorter (from 1950 to 1985) owing to the historical context of its recharge into the Big Aral Sea, which is also explained in the following quantitative analysis.

3 Results

3.1 Dynamics of the water volume change in the Aral Sea and its recharge runoff

3.1.1 Change point detection based on the BEAST model

The trend change point detection results for each variable (water volume change, Samanbay_R, K-S, K-K, Kelif_R, and Syr_Down_R) provided the number and year of change points as probabilities. The model results showed the probability of the number of change points for different variables. First, we selected all the numbers that had a probability greater than 0.100 (P>0.100). The water volume change showed the highest probability when it had 2 and 3 change points, with values equalling 0.532 and 0.326, respectively, and the 3 change points appeared in 1961 (P=0.725), 1974 (P=0.932), and 1992 (P=0.142). The Samanbay_R variable showed the highest probability when it had 1, 2, and 3 change points, with values equalling 0.387, 0.380, and 0.180, respectively, and the 3 change points occurred in 1961 (P=0.298), 1974 (P=0.939) and 1969 (P=0.074). The K-S variable also showed the highest probability when it had 1, 2, and 3 change points, with values of 0.397, 0.376, and 0.177, respectively, and the 3 change points appeared in 1961 (P=0.284), 1974 (P=0.931), and 1969 (P=0.073). The K-K variable had its highest probability with 2 and 3 change points, showing values of 0.856 and 0.101, respectively, and the 3 change points appeared in 1959 (P=0.953), 1981 (P=0.175), and 1991 (P=0.197). The Kelif_R variable exhibited the highest probability when it had 0, 1, and 2 change points, with values equalling 0.345, 0.370, and 0.159, respectively, and the 2 change points occurred in 1969 (P=0.084) and 1974 (P=0.106). Finally, the Syr_Down_R variable had the highest probability at 3 and 4 change points, with values of 0.774 and 0.210, respectively, and the 4 change points took place in 1957 (P=0.819), 1961 (P=0.991), 1965 (P=0.154), and 1974 (P=0.802). We further observed the change point years of each variable obtained from the initial screening, then eliminated the years with significantly lower probabilities, selected the years with significantly higher probabilities, and plotted them in Figure 3 (dashed line).

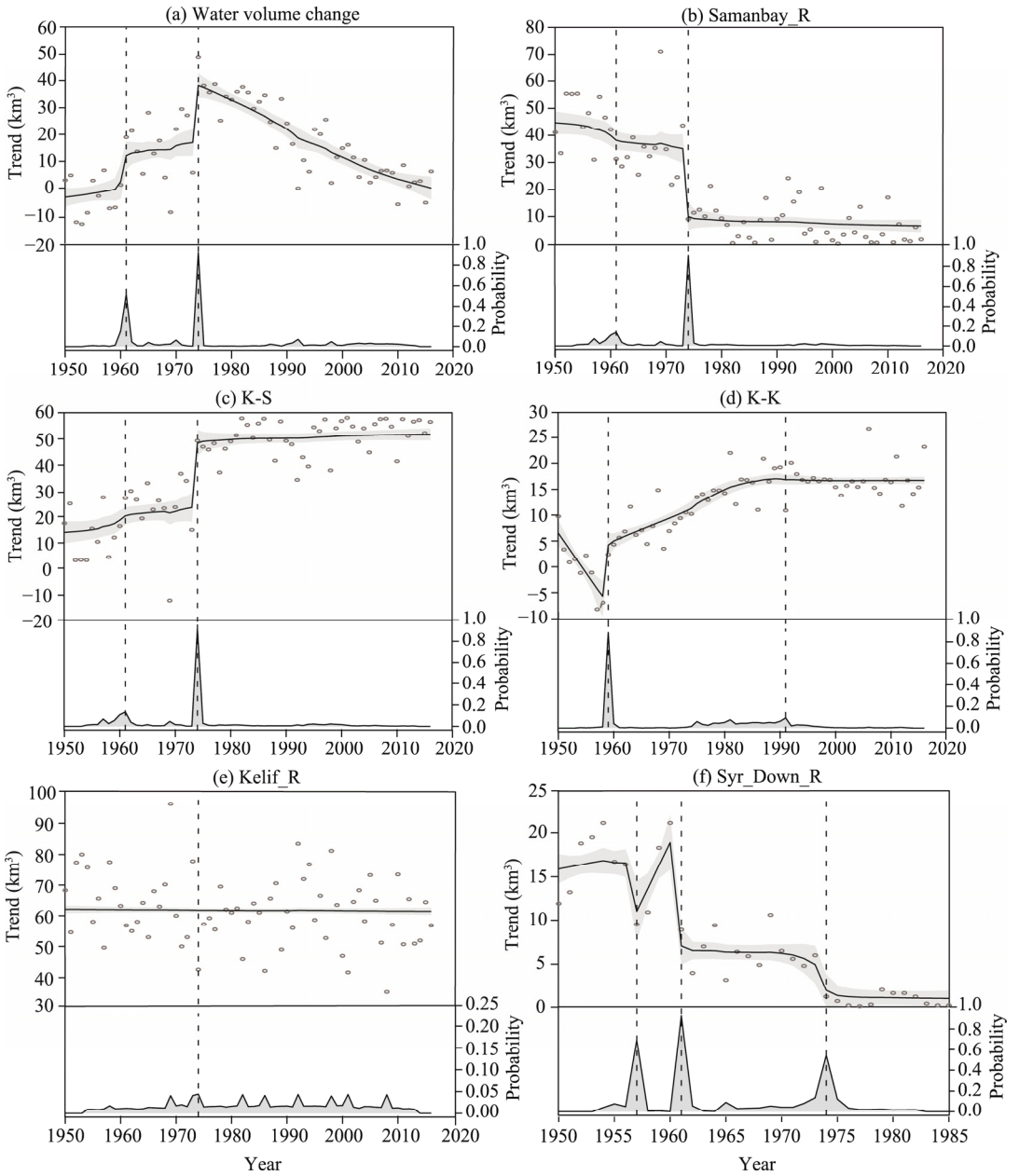

Fig. 3 Results of the change point detection for the study variables based on the Bayesian Estimator of Abrupt change, Seasonal change, and Trend (BEAST) model. (a), water volume change; (b), Samanbay_R (runoff from the downstream of the Amu Darya River); (c), K-S, water consumption in the middle-lower reaches of the Amu Darya River; (d), K-K, water consumption in the middle-upper reaches of the Amu Darya River; (e), Kelif_R, upstream-originating flow of the Amu Darya River; (f), Syr_Down_R, runoff from the downstream of the Syr Darya River. Dashed lines represent the location of change points, and grey envelopes indicate 95% credible intervals for the fitted trend signals.

The Samanbay_R and Syr_Down_R variables, representing the recharge runoff of natural channels in the Aral Sea, for the Amu Darya River and Syr Darya River, respectively, had the same change points as the water volume change in 1961 and 1974, showing a strong connection. The K-S and Samanbay_R variables showed high consistency in the change point detection results, denoting the high intensity of the connection. However, the results of the K-K variable completely differed from those of the Samanbay_R variable, and also did not present the same

change point years as the water volume change. This indicates that, compared with the K-S variable, the K-K variable had a smaller effect on the downstream runoff of the Amu Darya River and a weaker direct connection to the Aral Sea, suggesting that there may be more complex interactions; further argumentation may be given in the future. The Kelif_R variable had a change point year in 1974, as did the Samanbay_R variable and water volume change, but its occurrence probability value was rather low (only 0.106); therefore, even though a connection between them was evidenced, it was relatively weak. In summary, we found that years of 1961 and 1974 were not only the main trend change points of the dependent variable (water volume change), as seen in Figure 3, but also the years with the highest repetition rate and probability among the other variables, ranked the second and first, respectively. We used the stage division as the basis for further trend and statistical analyses.

3.1.2 Trend analysis and statistical characteristics by periods

We conducted trend (Table 1) and statistical (Table 2) analyses for each variable over three periods (1950–1960, 1961–1973, and 1974–2016). In periods one and two (1950–1960 and 1961–1973), all variables were stationary, but most showed distinctive statistical characteristics (including mean, minimum, and maximum values). Among them, the values for the water volume change, K-S variable, and K-K variable became larger during the transition from period one to period two, while variables Syr_Down_R and Samanbay_R displayed the opposite behaviour. In period three (1974–2016), the Syr_Down_R, K-K, and Kelif_R variables remained flat, but their specific values became smaller, larger, and smaller, respectively, compared to those in period two. The water volume change showed a significant downward trend with a P-value<0.01, a slope value of –1.032, and a mean value of 17.719 km^3/a. The Samanbay_R variable showed a weak downward trend with a P-value<0.05, a slope value of –0.175, and a mean value of 7.469 km^3. The K-S variable showed a weak upward trend with a P-value<0.05, a slope value of 0.175, and a mean value of 51.076 km^3. In particular, the K-K variable was further discussed in turn for other three periods: 1950–1958, 1959–1990, and 1991–2016, because of its distinctive trend characteristics. Specifically, it started with a non-stationary sequence in period one (1950–1958), showing a significant downward trend with a slope value of –1.746 and a mean value of 0.026 km^3. Then, it transitioned to another non-stationary sequence in period two (1959–1990), showing a significant upward trend with a slope value of 0.341 and a mean value of 11.709 km^3. Finally, it transitioned to a stationary sequence in period three (1974–2016), with a mean value of 16.973 km^3.

Table 1 Trend analysis of the variables by different periods and their slope values

Variable	1950–1960			1961–1973			1974–2016		
	Trend	Slope	P	Trend	Slope	P	Trend	Slope	P
WVC	→	-	-	→	-	-	↓	–1.032	***
Syr_Down_R	→	-	-	→	-	-	→	-	-
Samanbay_R	→	-	-	→	-	-	↓	–0.175	**
K-S	→	-	-	→	-	-	↑	0.175	**
K-K	→	-	-	→	-	-	→	-	-
Kelif_R	→	-	-	→	-	-	→	-	-
Variable	1950–1958			1959–1990			1991–2016		
	Trend	Slope	P	Trend	Slope	P	Trend	Slope	P
K-K	↓	–1.746	**	↑	0.341	***	→	-	-

Note: →, horizontal cyan arrow represents no significant upward or downward trend; ↑, upward red arrow represents an upward trend; ↓, downward purple arrow represents a downward trend; WVC represents the water volume change in the Aral Sea; Syr_Down_R, runoff from the downstream of the Syr Darya River; Samanbay_R, runoff from the downstream of the Amu Darya River; K-S, water consumption in the middle-lower reaches of the Amu Darya River; K-K, water consumption in the middle-upper reaches of the Amu Darya River; Kelif_R, upstream-originating flow of the Amu Darya River. ** indicates significant level at P<0.05 level; *** indicates significant level at P<0.01 level. -, no data.

Table 2 Statistical characteristics of the variables by different periods

Variable	1950–1960			1961–1973			1974–2016		
	Mean	Min	Max	Mean	Min	Max	Mean	Min	Max
WVC (km^3/a)	–3.103	–14.076	6.724	15.212	–6.112	30.570	17.719	–6.033	48.968
Syr_Down_R (km^3)	16.127	9.500	21.100	6.400	3.200	10.600	0.908	0.200	2.100
Samanbay_R (km^3)	45.994	31.005	55.400	35.059	21.818	71.067	7.469	0.117	24.196
K-S (km^3)	12.550	3.145	27.539	23.486	–12.523	36.727	51.076	34.348	58.427
K-K (km^3)	0.630	–8.200	9.756	7.948	3.527	14.836	16.295	10.224	26.723
Kelif_R (km^3)	67.182	49.600	80.000	63.485	50.000	96.300	59.837	35.300	83.500
Variable	1950–1958			1959–1990			1991–2016		
	Mean	Min	Max	Mean	Min	Max	Mean	Min	Max
K-K (km^3)	0.026	–8.200	9.756	11.709	2.375	22.005	16.973	11.750	26.723

Note: Min indicates minimum; Max indicates maximum.

3.2 Relationship between the water volume change in the Aral Sea and its recharge runoff

3.2.1 Non-linear cross-correlation based on the MF-DCCA

In this study, the MF-DCCA method was used to test the long-range cross-correlation of the water volume change with the variables of Samanbay_R, K-S, K-K, Kelif_R, Kerki_R, and water area, by obtaining the Hurst index at different q-values. As shown in Figure 4, where the horizontal axis is the q-value and the vertical axis is the Hurst index value, there was a large difference in the Hurst index obtained by the water volume change and each variable at different q-values, indicating multifractal characteristics in their mutual correlation. When q-values successively increased from –5 to 5, the Hurst index was different in the non-linear functions, indicating that there were different power-law relations between the water volume change and other variables. By comparing the variation range of these cross-correlation indices, we found that the cross-correlations between the water volume change and water area had the highest multifractal degree, while those between the water volume change and Kelif_R variable had the lowest multifractal degree. This indicates that the correlation between the water volume change and water area was the most complex and had the strongest linkage, while the correlation between the water volume change and Kelif_R variable was the simplest and weakest. This is attributed to the relationship between the water volume change and water area being both non-linear, as determined by topography, and also representing a joint response to the net water outflow from evaporation.

The lowest Hurst index values between the water volume change and Samanbay_R variable, between the water volume change and K-S variable, and between the water volume change and K-K variable were 0.66, 0.66, and 0.64, respectively. These values were all greater than 0.50, suggesting that there exists a long-range cross-correlation between them, regardless of the fluctuation magnitude; that is, when a sequence had a certain trend, another sequence was likely to show a synergistic trend. Of these, the variable pairs of the water volume change–Samanbay_R and water volume change–K-S not only had the smallest Hurst index values greater than 0.50, but also showed the same overlapping curve in Figure 4, proving that the Samanbay_R and K-S variables have mostly consistent synergistic effects on the water volume change.

However, the cross-correlation of the water volume change with the variables of Kelif_R, water area, and Kerki_R denoted a power-law relation that was completely different from that of the previous variables. When q-value<0, each cross-correlation index was smaller than 0.50, showing that the cross-correlation at smaller fluctuations was anti-persistent; that is, smaller changes between the water volume change and other variables were more likely to change in the opposite direction. When the Kelif_R variable showed a big upward trend, for example, there was a very likely sharp downward tendency in the water volume change, which was also consistent with the large increase in the upstream water supply and the slowing process of the Aral Sea shrinkage. When q-value>0, each cross-correlation index was larger than 0.50, showing that the

cross-correlation at larger fluctuations had a relatively long-range persistence. Namely, the large fluctuations in the water volume change would be affected by the long-term effects of the Kelif_R, Kerki_R, and water area, which were more likely to change in the same direction. For example, when water area showed a small upward (or downward) trend, the water volume change was also likely to demonstrate such a trend.

Additionally, we found that the water volume change and water area had the strongest and most complex long-range correlation. The long-range correlation of the water volume change with the Kelif_R variable, the Kerki_R variable, and the Samanbay_R variable, also successively strengthened. This may have been related to the growing geographical proximity to the Aral Sea. The persistent influence on the water volume change by the K-K variable and K-S variable showed the opposite state under different fluctuation amplitudes, which may related to the mechanism of their influence on the Aral Sea shrinkage. The water consumption of different reaches could not only directly affect the replenishment of water into the Aral Sea, but also indirectly impact the replenishment of water into the Aral Sea through the influence of human activities (e.g., irrigation). Consequently, various mechanisms produced different long-range effects.

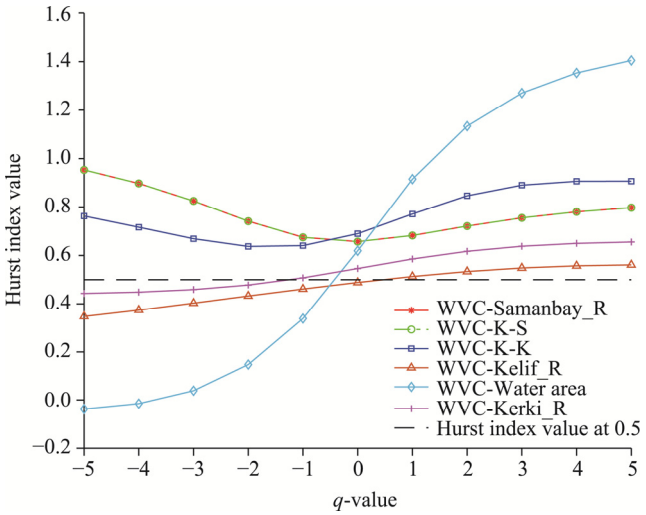

Fig. 4 Long-range cross-correlations of the water volume change (WVC) with different variables. *q*-value is the order of the fluctuation function that can be changed to examine different characteristics of the data.

3.2.2 Quantitative analysis

The model simulation results are presented in Tables 3 and 4. For Model I, by constructing the relationships of the water volume change with water area, Samanbay_R, and Syr_Down_R, and combining them with the theoretical capacity of the Aral Sea, we obtained quantitative relationships between the water volume of the Aral Sea and its recharge runoff during 1950–1985. The model was statistically significant, and each coefficient was reliable. As shown by the standardised coefficients, the relative importance of the net evaporation (represented by water area) and the recharge runoff of the Aral Sea (represented by the Samanbay_R and Syr_Down_R) to the Aral Sea shrinkage was 0.170, 0.741, and 0.401, respectively. Model II obtained quantitative relations between the water volume and the runoff in the Amu Darya River during 1986–2016 by constructing the relations of the water volume change with the water area and Samanbay_R. The model was statistically significant, and each coefficient was reliable. As can be seen from the standardised coefficients, the relative importance of the water area (net evaporation) and Samanbay_R to the Aral Sea shrinkage amounted to 0.647 and 0.690, respectively. Model III showed a quantitative relationship of the water volume with the runoff in the Amu Darya River and water consumption of the Amu Darya River during the 1986–2016 period by constructing the relationship of the water volume change with the water area, K-K, K-S, Kelif_R and THC_V. Overall, the model fitted well but the coefficients for the K-K were not

statistically significant, unlike the other coefficients. Therefore, the direct effect of the K-K during the 1986–2016 period was insignificant. We removed the K-K variable, continued the construction of the quantitative models, and obtained Model IV. Model IV was overall statistically significant, and its respective coefficients were reliable. The standardised coefficients showed that the relative importance of the net evaporation, water consumption of the Amu Darya River (excluding the reservoir water), THC_V, and Kelif_R to the shrinkage of the Aral Sea were 0.934, 0.705, 0.446, and 0.054, respectively.

Table 3 Specific structure and parameter estimates of Model I and Model II

	Model I (1950–1985)	Model II (1986–2016)
Formula	$\mathrm{WVC}=\alpha_1\times\mathrm{WA}-\beta_{11}\times R_1-\beta_2\times R_2$ $\mathrm{WA}=\begin{cases}0.08\times\mathrm{WV}-20.86, & \mathrm{WV}\in(961,1006]\\ -1.68\text{e-}05\times\mathrm{WV}^2+0.05\times\mathrm{WV}+22.52, & \mathrm{WV}\in(422,961]\end{cases}$	$\mathrm{WVC}=\alpha_2\times\mathrm{WA}-\beta_{12}\times R_1$ $\mathrm{WA}=\begin{cases}2.68\text{e}-9\times\mathrm{WV}^4+3.28\times\mathrm{WV}^3+1.59\text{e}-3\times\mathrm{WV}^2-0.41\times\mathrm{WV}+11.54, & \mathrm{WV}\in(79,422]\\ 3.97\text{e}-6\times\mathrm{WV}^4-1.04e-3\times\mathrm{WV}^3+0.10\times\mathrm{WV}^2-3.75\times\mathrm{WV}+51.31, & \mathrm{WV}\in[43,79]\end{cases}$
GOF	R^2=0.9212 Adjusted R^2=0.9164	R^2=0.9326 Adjusted R^2=0.9303

	Model I: parameter estimate			Model II: parameter estimate	
	α_1	β_{11}	β_2	α_2	β_{12}
Coef.	0.837***	–0.772***	–1.217***	0.864***	–0.964***
Std coef.	0.170**	–0.741***	–0.401**	0.647***	–0.690***

Note: GOF represents the goodness-of-fit of the model; Coef. represents the unstandardized coefficients for the multiple regression equations in the models; and Std coef. represents the standardised coefficients for the multiple regression equations in the models. WA represents the water area in the Aral Sea; R_1 represents the recharge runoff from the Amu Darya River; R_2 denotes the recharge runoff from the Syr Darya River; and α_1, α_2, β_{11}, β_{12}, and β_2 are the coefficients. ** indicates significant at P<0.05 level, and *** indicates significant at P<0.01 level.

Table 4 Specific structure and parameter estimates of Model III and Model IV

	Model III (1986–2016)	Model IV (1986–2016)
Formula	$\mathrm{WVC}=\alpha_3\times\mathrm{WA}-\gamma_1\times C_1-\gamma_2\times C_2-\gamma_3\times U-\gamma_4\times RV$ $\mathrm{WA}=\begin{cases}2.68\text{e}-9\times\mathrm{WV}^4+3.28\times\mathrm{WV}^3+1.59\text{e}-3\times\mathrm{WV}^2-0.41\times\mathrm{WV}+11.54, & \mathrm{WV}\in(79,422]\\ 3.97\text{e}-6\times\mathrm{WV}^4-1.04\text{e}-3\times\mathrm{WV}^3+0.10\times\mathrm{WV}^2-3.75\times\mathrm{WV}+51.31, & \mathrm{WV}\in[43,79]\end{cases}$	$\mathrm{WVC}=\alpha_3\times\mathrm{WA}-\gamma_2\times C_2-\gamma_3\times U-\gamma_4\times RV$ $\mathrm{WA}=\begin{cases}2.68\text{e}-9\times\mathrm{WV}^4+3.28\times\mathrm{WV}^3+1.59\text{e}-3\times\mathrm{WV}^2-0.41\times\mathrm{WV}+11.54, & \mathrm{WV}\in(79,422]\\ 3.97\text{e}-6\times\mathrm{WV}^4-1.04\text{e}-3\times\mathrm{WV}^3+0.10\times\mathrm{WV}^2-3.75\times\mathrm{WV}+51.31, & \mathrm{WV}\in[43,79]\end{cases}$
GOF	R^2=0.9074 Adjusted R^2=0.8931	R^2=0.9041 Adjusted R^2=0.8934

	Model III: parameter estimate					Model IV: parameter estimate			
	α_3	γ_1	γ_2	γ_3	γ_4	α_3	γ_2	γ_3	γ_4
Coef.	0.765***	0.201	0.360***	–0.348***	0.204**	0.768***	0.382***	–0.323***	0.246***
Std coef.	0.934***	0.010	0.705***	–0.054	0.446***	0.936***	0.713***	–0.045	0.454***

Note: C_1 represents the water consumption in the middle-upper reaches of the Amu Darya River (K-K); C_2 represents the water consumption in the middle-lower reaches of the Amu Darya River (K-S); U represents the upstream-originating flow of the Amu Darya River (Kelif_R); RV represents the water storage in the reservoir of the Tuyamuyun Hydro Complex (THC_V); and α_3, γ_1, γ_2, γ_3, and γ_4 are the coefficients.

In summary, during the 1950–1985 period, the Samanbay_R was the dominant factor affecting the Aral Sea shrinkage; the second was the Syr_Down_R, followed by the net evaporation. During 1986–2016, the water loss by net evaporation and the K-S were almost equally important to the water volume, even though net evaporation was far more influential than water use along

the river sections of the Amu Darya River. The importance of the variables affecting the Aral Sea followed an order of K-S>THC_V>Kelif_R>K-K.

4 Discussion

4.1 Historical evolution of the Aral Sea shrinkage and its causes

Based on the above analysis of trend change points, we discussed the evolutionary process of the Aral Sea in different time periods, as well as the changes in other hydrological process associated with it. By combining with key background events in the Aral Sea region during 1950–2016 period (Table 5), we explored the specific causes of the Aral Sea shrinkage.

From 1950 to 1960, the water volume change tended to be flat and showed a small negative value, implying a weak increasing trend in the water volume of the Aral Sea. However, this state was interrupted in 1961, after which the Aral Sea started to shrink, with a shrinkage rate fluctuating around 15.212 km^3/a. Correspondingly, the Samanbay_R and Syr_Down_R underwent abrupt changes in 1961, with a sudden decrease in runoff. The former had an average annual runoff value of 35.059 km^3 during 1961–1973, showing a decline of 10.935 km^3 from the previous time period, whereas the latter had an average annual value of 6.400 km^3, representing a decrease of 9.727 km^3 from the former time period. We believe that the abrupt decrease in the downstream of the recharging rivers during the 1960s caused the Aral Sea to shrink because the received recharge amount seemed insufficient to compensate the evaporation. This result is attributed to the large-scale development of irrigated agriculture in the Aral Sea region starting in the late 1950s (Aldaya et al., 2010; Bekchanov et al., 2012; Tischbein et al., 2012), when the Soviet government ordered a specialisation in cotton production. Consequently, the construction of the gigantic Karakum Canal began in 1954 and started working in 1956, drawing water from the Amu Darya River to Turkmenistan (Micklin and Aladinet al., 2008). After 1960, the amount of water used for irrigation increased (Spoor, 1993; Abduraupov et al., 2022), as did the irrigated area from approximately 4.510×10^4 km^2 in 1960 to about 5.150×10^4 km^2 in 1970.

The year 1974 represented the most significant change point in change point detections for all time series. During this year, the Aral Sea shrank at a rate of up to 48.968 km^3/a, which was the highest value measured in this study. Simultaneously, the Samanbay_R and Syr_Down_R plummeted to 9.049 and 1.300 km^3, respectively. The continued significant decrease in the flow of the two recharging rivers is believed to have caused a sudden and accelerated shrinkage of the Aral Sea, with the Samanbay_R and Syr_Down_R dropping by up to 26.010 and 5.100 km^3, respectively, compared to the average values registered during the 1961–1973 period. During the 1970s, irrigation technologies were greatly developed, and a large number of irrigation facilities were built in the Aral Sea region (Abdullaev, 2004). For example, the Karshi Canal and Amu-Bukhara Canal, two of the most important water diversions along the Amu Darya River, were put into operation in 1973 and 1974, respectively (corresponding to the change point year of 1973), with respective maximum flows of 160.000 and 360.000 m^3/s and average annual diversions of 4.000 and 4.500 km^3 (Schlüter et al., 2005). This suggests that there is a qualitative improvement in the efficiency of the local use of water resources. The large amount of water used for agriculture in the 1970s together with new land development schemes in the Hunger, Karshi, Dzhizak, and Sherabad steppes, the Karakum Canal, and Kyzylkum Canal (Dukhovny et al., 2007) led to the above-mentioned phenomenon, that is, a sharp decrease in the Samanbay_R and Syr_Down_R and a high rate of the shrinkage of the Aral Sea.

Following, the Syr_Down_R remained steady during the 1974–1985 period, while the Samanbay_R showed a weak and stable decreasing trend (a slope value of –0.175 km^3/a during the period 1974–2016), with a very small average value that can be explained by human activities at that time. The irrigated area in the Aral Sea region continued to grow in the 1980s but stagnated in the late 1990s, after which it stabilized at 8.000×10^4 km^2 (FAO, 2020). This is due to the collapse of the former Soviet Union in 1991, when the construction of a large number of irrigation facilities ceased, followed by a reduction in the cotton area and a decline in cotton production

(Spoor, 1998). Although the irrigated area ceased to grow significantly after the 1990s, the cropping structure began to shift, with wheat gradually replacing cotton as the main local crop (Abdullaev et al., 2005; Kariyeva and van Leeuwen, 2012; de Beurs et al., 2015), so agricultural water use continued to grow. For example, in Uzbekistan, the share of cotton in the total irrigated area significantly declined during the 1990s, while the share of grain crops increased. However, the shrinkage rate of the Aral Sea has been continuously decreasing, with a slope value of –1.032 km^3/a, implying that the Aral Sea continued to shrink at a gradually slower rate. This is because during this period, as the shrinking area of the Aral Sea was decreasing, evaporation also gradually declined, leading to a gradual drop in the shrinkage rate and a continuous advance towards the Aral Sea, achieving re-equilibrium (i.e., the evaporation and recharge were nearly equal). At this stage, the importance of net evaporation for the evolution of the Aral Sea began to emerge, though it has been ignored in most existing studies (Yang et al., 2020b; Li et al., 2021; Su et al., 2021; Shi et al., 2022).

Because the Samanbay_R was determined by the amount of incoming upstream-originating flow and the amount of water consumed by each river section, the Kelif_R, K-K, and K-S variables were considered in this study. Considering the described results, the trend of the Kelif_R was relatively stable, without evident upward or downward trends. The K-S variable kept rising during three periods (1950–1961, 1962–1973, and 1974–2016), with a rising proportion in the total water consumption. Meanwhile, the magnitude of the K-K variable was much smaller than that of the K-S variable, and the change point years of the K-K variable were completely different from those of the water volume change variable, meaning that its influence on the Aral Sea was not as strong as that of the K-S variable. Therefore, we believe that the K-S was the main reason for the variation of the Samanbay_R. Moreover, the results of the change point and long-range cross-correlation analyses were consistent with the Samanbay_R variable, with the same change points (in 1961 and 1974, respectively) and long-range correlation curve.

Table 5 List of the background events in the Area Sea region during 1950–2016 period

	1950–1960	1961–1973	1974–1991	1992–2016
Events	(1) The Soviet government ordered the large-scale cotton production in the late 1950s. (2) The construction of the Karakum Canal began in 1954, and was put into operation in 1956.	(1) From 1960 to 1970, the irrigated area in the Aral Sea region experienced an approximate increase of 6.400×10^3 km^2.	(1) The Karshi Canal began its operation in 1973. (2) The Amu-Bukhara Canal was put into use in 1974. (3) The cotton-growing area in the Aral Sea region reached a stable state in the 1980s.	(1) The Soviet Union dissolved in 1991. (2) Around 1992, significant changes occurred in the cropping structure, with the cotton area decreasing and the area of grain crops increasing.

4.2 Exploring the response of the Aral Sea to human activities by scenario analysis

Using various historical water use scenarios, the evolution of the Aral Sea under different scenarios was simulated to better understand the impact of different water use policies. According to the water use analysis and purpose of this study, combined with existing studies (Froebrich and Kayumov, 2004; Sun et al., 2019; Yuldashev et al., 2020), it should be possible to increase the water coming from the lower reaches of the Amu Darya River to different degrees of the water level in 1961–1973 by increasing the efficiency of agricultural water use and reducing it in the middle and lower reaches, thereby reducing ineffective evaporation from reservoirs and wetlands. Thus, we set up three scenarios: Scenario 1, after 1974, with the Samanbay_R without a cliff drop and maintaining the flow level of 1961–1973 in the previous period (i.e., the water consumption of the river section (upstream of the Samanbay hydrological station) maintained the flow level of 1961–1973 during 1974–2016); Scenario 2, compared to the flow level during the period 1974–2016 under Scenario 1 with a 100% recovery, it is assumed that the Samanbay_R recovered by 50% after 1974 (1974–2016); and Scenario 3, assuming that no THC reservoir (in-channel) was historically built (it was actually constructed in 1983), namely, the water consumption of the

river section (upstream of the Samanbay hydrological station) continued to maintain the same level during the historical period of 1974–1982. Scenarios 1 and 2 were assumptions about whether agriculture expanded along the Amu Darya River after 1974 and to what extent. Contrastingly, Scenario 3 was designed to explore whether the reservoir water storage had an effect on the Aral Sea. The Samanbay_R during 1974–2016 period was 100%, 50%, and approximately 30% of the flow level during 1961–1973 period under the Scenario 1, Scenario 2, and Scenario 3, respectively (Fig. 5).

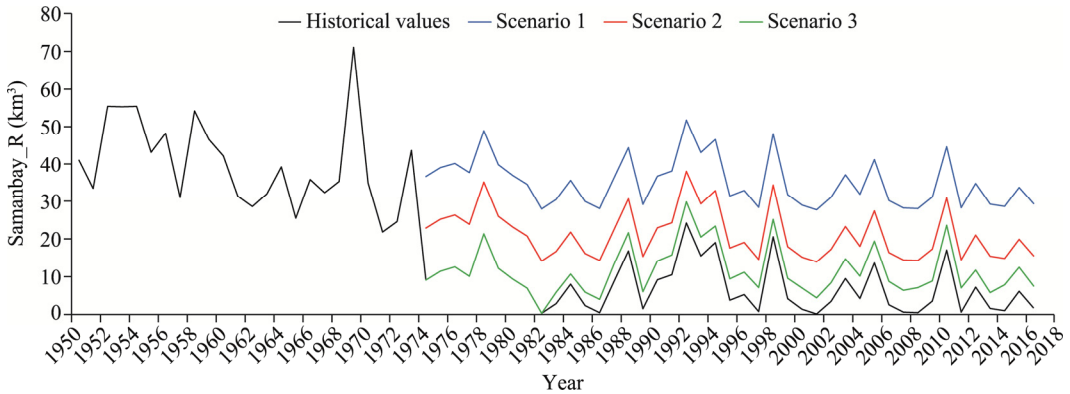

Fig. 5 Comparison between historical runoff values in the downstream of the Amu Darya River and simulated runoff values under different scenarios

Through the joint simulation of Model I and Model II shown above, we obtained the evolutionary process of the water volume in the Aral Sea under the three scenarios (Fig. 6).

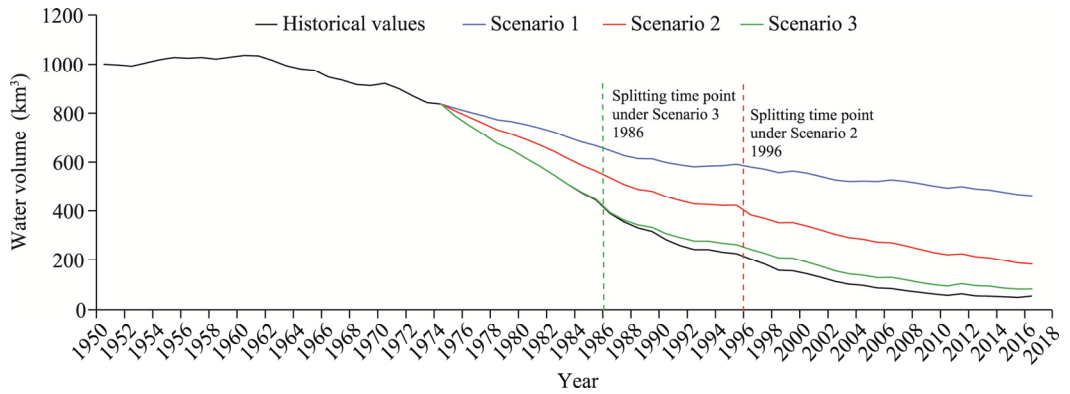

Fig. 6 Comparison between historical water volume values in the Aral Sea and simulated water volume values under different scenarios

Under Scenario 1, after 1974, the Samanbay_R remained consistent with the previous level (average annual value of 35.060 km^3 during 1961–1973), while the total annual water consumption of the Amu Darya River was approximately 24.778 km^3. In this case, during the evolution of the Aral Sea, demonstrated by the blue line, the water volume decreased slowly, from 843.023 km^3 in 1973 to 666.693 km^3 in 1985 (221.987 km^3 higher than the historical value of 444.706 km^3), until it fell to 462.185 km^3 in 2016, well above the historical value (54.561 km^3). There was no split since then. Under Scenario 2, after 1974, when the Samanbay_R was maintained at an average annual level of approximately 21.264 km^3, the total annual water consumption of the Amu Darya River was approximately 38.573 km^3. In this case, the water volume of the Aral Sea gradually decreased from 843.023 km^3 in 1973 to 383.803 km^3 in 1996, leading the Aral Sea dividing into the Big Aral Sea and Small Aral Sea, with a 10-year delay

compared with history (1986). Additionally, by 2016, water volume decreased to 183.552 km^3. Under Scenario 3, the THC reservoir was no longer constructed in 1983 and the Samanbay_R maintained the average annual level of approximately 10.351 km^3 prior to 1983; that is, the total annual water consumption of the Amu Darya River measured approximately 46.916 km^3. In this case, the water volume rapidly decreased from 843.023 km^3 in 1973 to 394.062 km^3 in 1986, when the Aral Sea was divided into the Big Aral Sea and Small Aral Sea. This time point was consistent with history, showing that the suspension of the THC reservoir in 1983 could not change the evolution of the Aral Sea, as indicated in Figure 6. After the division of the Aral Sea in 1986, from 1986 to 2016, the water volume of the Aral Sea was slightly larger than the historical water amount (approximately 33.583 km^3), and the water volume fell to 83.251 km^3 until in 2016.

5 Conclusions

The famous Aral Sea crisis in the arid zone of Central Asia, which poses huge pressures on the local ecology and sustainable development, is mainly attributed to the excessive exploitation of water resources in the Amu Darya River by human activities. In this study, we applied the BEAST model to detect the trend change points of involved variables, discussed the non-linear relationships between the Aral Sea's water volume and Amu Darya River's runoff using the MF-DCCA method, and provided their quantitative correlations. On this basis, we explored the evolution of the Aral Sea during the 1950–2016 period and analysed the causes of its shrinkage over different time periods. Additionally, we explored how the Amu Darya River affected the Aral Sea both historically and under different scenarios. The main conclusions are as follows:

(1) During the 1950–2016 period, the water volume change of the Aral Sea had two significant trend change points in 1961 and 1974. Simultaneously, other hydrological variables linked to the Aral Sea, of which, the Samanbay_R, Syr_Down_R, and K-S, showed the same trend change points in 1961 and 1974, the Kelif_R variable had only one weak trend change point in 1961, whereas the K-K variable had two completely different trend change points, in 1959 and 1991. These change points, corresponding to significant changes in time series data, help reveal the state of the Aral Sea and the identified variables during different periods. The years of 1961 and 1974, frequently appeared in various related variables, implying their strong correlation between each other.

(2) The long-range cross-correlation between the water volume change of the Aral Sea and the related variables (Samanbay_R, Kerki_R, Kelif_R, K-S, K-K, and water area) showed multifractal characteristics. The water volume change showed long-range cross-correlations with the Samanbay_R, K-S, and K-K variables consistently, regardless of the fluctuation magnitude. The water volume change only had long-range cross-correlations at larger fluctuations with the Kerki_R, Kelif_R, and water area variables. Finally, the Samanbay_R and K-S variables had mostly consistent synergistic effects on the water volume change.

(3) Before 1974, the Samanbay_R was the dominant factor affecting the Aral Sea shrinkage, followed by the Syr_Down_R and the net evaporation. From 1974, the importance of net evaporation began to appear, and after 1986, its impact on the Aral Sea was almost as important as the recharge water of Samanbay_R, even though it was far more influential than water use along the river sections of the Amu Darya River. In summary, the decrease in the Samanbay_R was the main cause of the Aral Sea shrinkage, and the K-S was the main reason for the variation in the Samanbay_R. The order of importance of the variables in the Amu Darya River system affecting the Aral Sea shrinkage is as follows: K-S>THC_V>Kelif_R>K-K.

(4) This study evaluates the evolution of the Aral Sea under different scenarios and compares it with the historical evolution process. It was found that when the Samanbay_R during the 1974–2016 period recovers by 50% of the 1961–1973 level, the Aral Sea would split in 1996, which is a decade later than the historical split in 1986. Thus, it is possible to slow down the retreat of the Aral Sea and stabilize its water area and water volume in an ecologically restored

state, when recovering the Samanbay_R after 1974 to the 1961–1973 level, by increasing the efficiency of agricultural water use, reducing agricultural water use in the middle and lower reaches, and reducing ineffective evaporation from reservoirs and wetlands.

This study examined the relationship between the Aral Sea shrinkage and the runoff of the Amu Darya River in detail and offers new perspectives on the causes of shrinkage in the Aral Sea. However, further improvement is required, and more human activity factors and human policies on water and land use should be taken into consideration in the future.

Conflict of interest

The authors declare that they have no known competing financial interests or personal relationships that could have appeared to influence the work reported in this paper.

Acknowledgements

This research was supported by the National Natural Science Foundation of China (42230708), the Joint CAS (Chinese Academy of Sciences) & MPG (Max-Planck-Gesellschaft) Research Project (HZXM20225001MI), and the Tianshan Talent Project of Xinjiang Uygur Autonomous Region, China (2022TSYCLJ0056). The authors are grateful to the editors and anonymous reviewers for their insightful comments and suggestions.

Author contributions

Conceptualization: WANG Min, CHEN Xi; Data curation: WANG Min, CAO Liangzhong, SHI Haiyang, WU Nannan; Methodology: WANG Min; Formal analysis: WANG Min, CHEN Xi; Writing - original draft preparation: WANG Min, CHEN Xi, KURBAN Alishir, EZIZ Anwar, YUAN Xiuliang; Writing - review and editing: WANG Min, CAO Liangzhong, SHI Haiyang; Funding acquisition: CHEN Xi, Philippe DE MAEYER; Supervision: CHEN Xi, Philippe DE MAEYER.

References

Abdullaev I. 2004. The analysis of water management in Bukhara oasis of Uzbekistan: historical and territorial trends. Water International, 29(1): 20–26.

Abdullaev I, Giordano M, Rasulov A. 2005. Cotton in Uzbekistan: Water and Welfare. In: Proceedings of Conference on "Cotton Sector in Central Asia: Economic Policy and Development Challenges". 3–4 November, 2005. The School of Oriental and African Studies, University of London, London.

Abduraupov R, Akhmadjanova G, Ibragimov A, et al. 2022. Modeling of water management for cotton production in Uzbekistan. Agricultural Water Management, 265: 107535, doi: 10.1016/j.agwat.2022.107535.

Aldaya M M, Muñoz G, Hoekstra A Y. 2010. Water Footprint of Cotton, Wheat and Rice Production in Central Asia. Research Report Series No. 41. Delft, The Netherlands: UNESCO-IHE Institute for Water Education.

Alkan Ç, Konukcu F. 2022. An investigation on the climate change and drought types in the Porsuk Stream Watershed, west of Turkey. Algerian Journal of Engineering and Technology, 7: 37–46.

Bai J, Chen X, Yang L, et al. 2012. Monitoring variations of inland lakes in the arid region of Central Asia. Frontiers of Earth Science, 6: 147–156.

Banakara K B, Sharma N, Sahoo S, et al. 2023. Evaluation of weather parameter-based pre-harvest yield forecast models for wheat crop: a case study in Saurashtra region of Gujarat. Environmental Monitoring and Assessment, 195: 51, doi: 10.1007/s10661-022-10552-4.

Bekchanov M, Lamers J P A, Karimov A, et al. 2012. Estimation of spatial and temporal variability of crop water productivity with incomplete data. In: Martius C, Rudenko I, Lamers J P A, et al. Cotton, Water, Salts and Soums. Dordrecht: Springer, 329–344.

Berdugo M, Gaitán J J, Delgado-Baquerizo M, et al. 2022. Prevalence and drivers of abrupt vegetation shifts in global drylands. Proceedings of the National Academy of Sciences, 119(43): e2123393119, doi: 10.1073/pnas.2123393119.

Cai D L, Yu L J, Zhu J F, et al. 2022. The shrinkage of Lake Lop Nur in the twentieth Century: A comprehensive ecohydrological analysis. Journal of Hydrometeorology, 23(8): 1245–1255.

Chen S A, Michaelides K, Grieve S W D, et al. 2019. Aridity is expressed in river topography globally. Nature, 573: 573–577.

de Beurs K M, Henebry G M, Owsley B C, et al. 2015. Using multiple remote sensing perspectives to identify and attribute land

surface dynamics in Central Asia 2001–2013. Remote Sensing of Environment, 170: 48–61.
Dukhovny V, Umarov P, Yakubov H, et al. 2007. Drainage in the Aral Sea basin. Irrigation and Drainage, 56(S1): S91–S100.
FAO (Food and Agriculture Organization of the United Nations). 2020. FAOSTAT data. [2023-01-30]. http://faostat.fao.org.
Feng Y H, Zhang H, Tao S L, et al. 2022. Decadal lake volume changes (2003–2020) and driving forces at a global scale. Remote Sensing, 14(4): 1032, doi: 10.3390/rs14041032.
Foster S. 2018. Is UN Sustainable Development Goal 15 relevant to governing the intimate land-use/groundwater linkage? Hydrogeology Journal, 26(4): 979–982.
Froebrich J, Kayumov O. 2004. Water management aspects of Amu Darya: Options for future strategies. In: Nihoul J C J, Zavialov P O, Micklin P P. Dying and Dead Seas Climatic Versus Anthropic Causes. NATO Science Series: IV: Earth and Environmental Sciences. Dordrecht: Springer, 49–76.
Fróna D, Szenderák J, Harangi-Rákos M. 2021. Economic effects of climate change on global agricultural production. Nature Conservation, 44: 117–139.
Grant L, Vanderkelen I, Gudmundsson L, et al. 2021. Attribution of global lake systems change to anthropogenic forcing. Nature Geoscience, 14(11): 849–854.
He H L, Hamdi R, Luo G P, et al. 2022. Numerical study on the climatic effect of the Aral Sea. Atmospheric Research, 268: 105977, doi: 10.1016/j.atmosres.2021.105977.
Hrvatin M, Zorn M. 2022. Climate change impacts on hydrology in the Mediterranean part of Slovenia. In: Leal Filho W, Manolas E. Climate Change in the Mediterranean and Middle Eastern Region. Cham: Springer, 85–118.
Hu Z Y, Chen X, Zhou Q M, et al. 2022. Dynamical variations of the terrestrial water cycle components and the influences of the climate factors over the Aral Sea Basin through multiple datasets. Journal of Hydrology, 604: 127270, doi: 10.1016/j.jhydrol.2021.127270.
Huang J P, Yu H P, Guan X D, et al. 2016. Accelerated dryland expansion under climate change. Nature Climate Change, 6(2): 166–171.
Huang W J, Duan W L, Chen Y N. 2022. Unravelling lake water storage change in Central Asia: Rapid decrease in tail-end lakes and increasing risks to water supply. Journal of Hydrology, 614: 128546, doi: 10.1016/j.jhydrol.2022.128546.
Kariyeva J, van Leeuwen W J D. 2012. Phenological dynamics of irrigated and natural drylands in Central Asia before and after the USSR collapse. Agriculture, Ecosystems & Environment, 162: 77–89.
Kojić M, Schlüter S, Mitić P, et al. 2022. Economy-environment nexus in developed European countries: Evidence from multifractal and wavelet analysis. Chaos, Solitons and Fractals, 160: 112189, doi: 10.1016/j.chaos.2022.112189.
Konapala G, Mishra A K, Wada Y, et al. 2020. Climate change will affect global water availability through compounding changes in seasonal precipitation and evaporation. Nature Communications, 11: 3044, doi: 10.1038/s41467-020-16757-w.
Li Q, Li X, Ran Y H, et al. 2021. Investigate the relationships between the Aral Sea shrinkage and the expansion of cropland and reservoir in its drainage basins between 2000 and 2020. International Journal of Digital Earth, 14(6): 661–677.
Li Y, Qi S, Li J J. 2022. Research on ecological restoration technology in arid or semi-arid areas from the perspective of the Belt and Road Initiative. Journal of Resources and Ecology, 13(6): 964–976.
Liu H J, Chen Y N, Ye Z X, et al. 2019. Recent lake area changes in Central Asia. Scientific Reports, 9: 16277, doi: 10.1038/s41598-019-52396-y.
Liu Z B, Liu T, Huang Y, et al. 2022. Comparison of crop evapotranspiration and water productivity of typical delta irrigation areas in Aral Sea Basin. Remote Sensing, 14(2): 249, doi: 10.3390/rs14020249.
Micklin P P. 1988. Desiccation of the Aral Sea: a water management disaster in the Soviet Union. Science, 241(4870): 1170–1176.
Micklin P. 2007. The Aral Sea disaster. Annual Review of Earth and Planetary Sciences, 35: 47–72.
Micklin P, Aladin N V. 2008. Reclaiming the Aral Sea. Scientific American, 298(4): 64–71.
Micklin P. 2010. The past, present, and future Aral Sea. Lakes & Reservoirs: Research and Management, 15(3): 193–213.
Micklin P. 2016. The future Aral Sea: hope and despair. Environmental Earth Sciences, 75: 844, doi: 10.1007/s12665-016-5614-5.
Pettitt A N. 1979. A non-parametric approach to the change-point problem. Journal of the Royal Statistical Society: Series C (Applied Statistics), 28(2): 126–135.
Pham-Duc B, Sylvestre F, Papa F, et al. 2020. The Lake Chad hydrology under current climate change. Nature Scientific Reports, 10: 5498, doi: 10.1038/s41598-020-62417-w.
Pohlert T, 2016. Non-parametric trend tests and change-point detection. CRAN Repository. [2022-09-18]. https://CRAN.R-project.org/package=trend.
Rahmani F, Fattahi M H. 2021. A multifractal cross-correlation investigation into sensitivity and dependence of meteorological

and hydrological droughts on precipitation and temperature. Natural Hazards, 109(3): 2197–2219.

Rufin P, Peña-Guerrero M D, Umirbekov A, et al. 2022. Post-Soviet changes in cropping practices in the irrigated drylands of the Aral Sea basin. Environmental Research Letters, 17(9): 095013, doi: 10.1088/1748-9326/ac8daa.

Schlüter M, Savitsky A G, McKinney D C, et al. 2005. Optimizing long-term water allocation in the Amudarya River delta: a water management model for ecological impact assessment. Environmental Modelling & Software, 20(5): 529–545.

Sharma A, Huang H P, Zavialov P, et al. 2018. Impact of desiccation of Aral Sea on the regional climate of Central Asia using WRF model. Pure and Applied Geophysics, 175(1): 465–478.

Shi J C, Guo Q Z, Zhao S, et al. 2022. The effect of farmland on the surface water of the Aral Sea Region using Multi-source Satellite Data. PeerJ, 10: e12920, doi: 10.7717/peerj.12920.

Spoor M. 1993. Transition to market economies in former Soviet Central Asia: Dependency, cotton and water. The European Journal of Development Research, 5(2): 142–158.

Spoor M. 1998. The Aral Sea Basin crisis: transition and environment in former Soviet Central Asia. Development and Change, 29(3): 409–435.

Su Y N, Li X, Feng M, et al. 2021. High agricultural water consumption led to the continued shrinkage of the Aral Sea during 1992–2015. Science of The Total Environment, 777: 145993, doi: 10.1016/j.scitotenv.2021.145993.

Sun J, Li Y P, Suo C, et al. 2019. Impacts of irrigation efficiency on agricultural water-land nexus system management under multiple uncertainties—A case study in Amu Darya River basin, Central Asia. Agricultural Water Management, 216: 76–88.

Tischbein B, Awan U K, Abdullaev I, et al. 2012. Water management in Khorezm: Current situation and options for improvement (hydrological perspective). In: Martius C, Rudenko I, Lamers J P A, et al. Cotton, Water, Salts and Soums. Dordrecht: Springer, 69–92.

Vinushree R, Ashalatha K V, Mohammed Rizwan Saif, et al. 2022. Trend analysis of groundwater level using Mann-Kendall test in Dharwad district. The Pharma Innovation Journal, 11(5S): 596–600.

Wang J D, Song C Q, Reager J T, et al. 2018. Recent global decline in endorheic basin water storages. Nature Geoscience, 11(12): 926–932.

Wang X X, Chen Y N, Li Z, et al. 2020. The impact of climate change and human activities on the Aral Sea Basin over the past 50 years. Atmospheric Research, 245: 105125, doi: 10.1016/j.atmosres.2020.105125.

Woolway R I, Kraemer B M, Lenters J D, et al. 2020. Global lake responses to climate change. Nature Reviews Earth & Environment, 1(8): 388–403.

Wu Q Y, Yue H, Liu Y, et al. 2022. Geospatial quantitative analysis of the Aral Sea Shoreline changes using RS and GIS techniques. Earth Science Informatics, 15(1): 137–149.

Xiang C H, Hao X Z, Wang W H, et al. 2019. Asymmetric MF-DCCA method based on fluctuation conduction and its application in air pollution in Hangzhou. Journal of Advanced Computational Intelligence and Intelligent Informatics, 23(5): 823–830.

Yan X, Li L H. 2023. Spatiotemporal characteristics and influencing factors of ecosystem services in Central Asia. Journal of Arid Land, 15(1): 1–19.

Yang X C, Tian S Y, You W, et al. 2021. Reconstruction of continuous GRACE/GRACE-FO terrestrial water storage anomalies based on time series decomposition. Journal of Hydrology, 603: 127018, doi: 10.1016/j.jhydrol.2021.127018.

Yang X W, Wang N L, Chen A A, et al. 2020a. The relationship between area variation of the Aral Sea in the arid Central Asia and human activities and climate change. Journal of Glaciology and Geocryology, 42(2): 681–692. (in Chinese)

Yang X W, Wang N L, CHEN A A, et al. 2020b. Changes in area and water volume of the Aral Sea in the arid Central Asia over the period of 1960–2018 and their causes. CATENA, 191: 104566, doi: 10.1016/j.catena.2020.104566.

Yuldashev N K, Nabokov V I, Nekrasov K V, et al. 2020. Modernization and intensification of agriculture in the republic of Uzbekistan. E3S Web of Conferences, 222: 06033, doi: 10.1051/e3sconf/202022206033.

Zhang M, Chen Y N, Shen Y J, et al. 2019. Tracking climate change in Central Asia through temperature and precipitation extremes. Journal of Geographical Sciences, 29(1): 3–28.

Zhang Q F, Chen Y N, Li Z, et al. 2022. Controls on alpine lake dynamics, Tien Shan, Central Asia. Remote Sensing, 14(19): 4698, doi: 10.3390/rs14194698.

Zhao J S, Wang Z J, Weng W B. 2004. Study on the holistic model for water resources system. Science in China Series E: Technological Sciences, 47(1): 72–89.

Zhao K G, Wulder M A, Hu T X, et al. 2019. Detecting change-point, trend, and seasonality in satellite time series data to track abrupt changes and nonlinear dynamics: A Bayesian ensemble algorithm. Remote Sensing of Environment, 232: 111181, doi: 10.1016/j.rse.2019.04.034.